Assessing the work budget and efficiency of fault systems using mechanical models

Michele L. Cooke and Susan Murphy

Geosciences Department, University of Massachusetts, Amherst, Massachusetts, USA

Received 7 January 2004; revised 13 July 2004; accepted 26 July 2004; published 16 October 2004.

[1] We examine the work energy budget of actively deforming fault systems in order to develop a means of examining the systemic behavior of complex fault networks. Work done in the deformation of a faulted area consists of five components: (1) work done against gravity in uplift of topography (W_{grav}); (2) internal energy of the strained host rock (W_{int}); (3) work done resisting friction during slip on faults (W_{fric}); (4) seismic energy released in earthquake events as ground shaking (W_{seis}); and (5) work done in initializing new faults and propagating existing faults (W_{prop}). The energy budget of a fault system can be expressed as $W_{TOT} = W_{grav} + W_{int} + W_{fric} + W_{seis} + W_{prop}$. For a balanced energy budget the total of these five components will equal the external tectonic work applied to the system. We examine the work balance within hypothetical and simulated two-dimensional static fault systems using mechanical models. The boundary element method models produce a balanced work budget for both simple and complex fault system models. The presence of slipping faults reduces the internal strain energy of the faulted area (W_{int}), at a "cost" of work done against friction and gravity (and propagation and seismic energy, where applicable). Calculations of minimum work deformation match expected deformation paths, indicating the usefulness of this approach for evaluating efficiency in more complex systems. The partitioning of various work terms may express the relative efficiency or maturity of fault systems. Furthermore, calculation of potential seismic energy release can provide an upper bound to earthquake seismic moment assessments. *INDEX TERMS:* 8010 Structural Geology: Fractures and faults; 8020 Structural Geology: Mechanics; 8123 Tectonophysics: Dynamics, seismotectonics; 8122 Tectonophysics: Dynamics, gravity and tectonics; *KEYWORDS:* work minimization, fault system growth, mechanical models

Citation: Cooke, M. L., and S. Murphy (2004), Assessing the work budget and efficiency of fault systems using mechanical models, *J. Geophys. Res.*, *109*, B10408, doi:10.1029/2004JB002968.

1. Introduction

[2] Geologic faults rarely occur in isolation but develop within interacting systems of faults. Consequently, understanding the behavior (i.e., slip distribution, slip rates and growth) of any one fault requires consideration of the entire system. Field and numerical studies have shown that interacting faults have slip distributions different from those along equivalent isolated faults [*Willemse and Pollard*, 2000; *Maerten et al.*, 1999; *Savage and Cooke*, 2004]. Such differences may have important implications for the prediction of seismic hazards and understanding fault system evolution. Earthquake triggering studies, for example, have demonstrated that an earthquake on one fault can change the probability of earthquakes on nearby faults [e.g., *King et al.*, 1994; *Harris*, 1998; *Stein*, 1999]. Other studies have shown that fault systems evolve through the growth, interaction and linkage of individual fault segments [e.g., *Gupta et al.*, 1998; *Dawers and Underhill*, 2000; *Kattenhorn and Pollard*, 2001; *Mansfield and Cartwright*, 2001; *Childs et al.*, 2003].

0148-0227/04/2004JB002968$09.00

[3] We explore a method for analysis of an entire system of faults based on the work budget of the fault system. The distribution of work energy among forms of deformation, such as internal strain in the surrounding rock, topographic uplift, frictional slip and creation of new fault surfaces, can aid our understanding of the mechanical behavior and evolution of a fault system as a whole. For example, new fault surfaces develop at a work energy "cost" that must be compensated for, either in terms of reduced internal strain or an increase in the total tectonic work input into the system. The total work for each form of deformation provides a quantitative means to assess the behavior of the entire fault system. In this way, locally destructive or constructive fault interactions may be tempered by their role within the larger system. Investigation of work within a system of active faults assesses behavior that pertains to timescales that bridge those of single earthquakes and geologic deformation, thus providing critical insight into behavior of active fault systems.

1.1. Work Budget and Efficiency

[4] Work analyses of geologic processes have often been applied to assess the relative efficiency of alternative paths

of deformation [*Masek and Duncan*, 1998; *Jamison*, 1993; *Dahlen and Barr*, 1989; *Molnar and Lyon-Caen*, 1988; *Mitra and Boyer*, 1986; *Sleep et al.*, 1979]. These efficiency-based or minimum work analyses rely on the proposition that deformation will occur to minimize the work required to accommodate the tectonic strain. The work budgets of deforming fold-and-thrust belts have been analyzed by analogy to wedges of soil or snow that deform in front of a moving bulldozer; these analyses utilize the premise that the deforming wedge grows by minimizing the work done [*Dahlen and Barr*, 1989]. *Mitra and Boyer* [1986] used a minimum work criterion to assess the tendency of foreland duplexes to deform via slip on existing faults or by creation of new faults. *Jamison* [1993] relied on minimum work to explain the conditions under which triangle zones will form. *Masek and Duncan* [1998] explored the effect of friction and topography on the evolution of orogenic zones using minimum work techniques. Minimum work analyses have also been applied to predict the orientation of spreading ocean ridges and transforms [*Sleep et al.*, 1979] and explain the lateral expansion of continental platforms [*Molnar and Lyon-Caen*, 1988]. Our mechanical analysis, based on the approach of *Mitra and Boyer* [1986], extends from previous work by (1) including work components directly related to fault slip, such as strain concentration around fault tips and energy released in earthquakes, and (2) permitting evaluation of complexly interacting fault systems that are difficult to evaluate using the analytical methods cited above.

[5] Elements of a fault system's work budget, such as internal strain energy, have been used in conjunction with geologic data to evaluate between alternative fault systems [*Cooke and Kameda*, 2002; *Griffith and Cooke*, 2004]. However, these studies considered neither the inelastic components of several work terms nor the gravitational work of fault systems. Our rigorous balance of work budget components presented here provides a more complete tool for the analysis of alternative fault systems as well as fault system evolution.

[6] This paper presents each of the terms in the work budget, followed by two-dimensional analysis of an isolated single fault and a simple two-fault system under horizontal contraction. After building our intuition with the single-fault and two-fault models, we apply the work budget to the complexly interacting faults of the Los Angeles basin with a two-dimensional analysis. The insights gained by these two-dimensional analyses can also be applied to three-dimensional systems, although such applications are beyond the scope of this paper.

2. Work Budget of a Fault System

[7] Work done in the deformation of a faulted area consists of five components, shown in Figure 1 for the case of an idealized single fault system undergoing contraction. First, work is done against gravity in uplift of topography (W_{grav}). This term can be negative where deformation decreases elevation. Second, work is done in straining the host rock surrounding the fault. We refer to this work as the internal strain energy (W_{int}). Third, when a fault slips, work is done resisting friction along the fault surface (W_{fric}). Heat energy resulting from frictional slip is taken into account within the W_{fric} term. W_{fric} will be zero for a frictionless

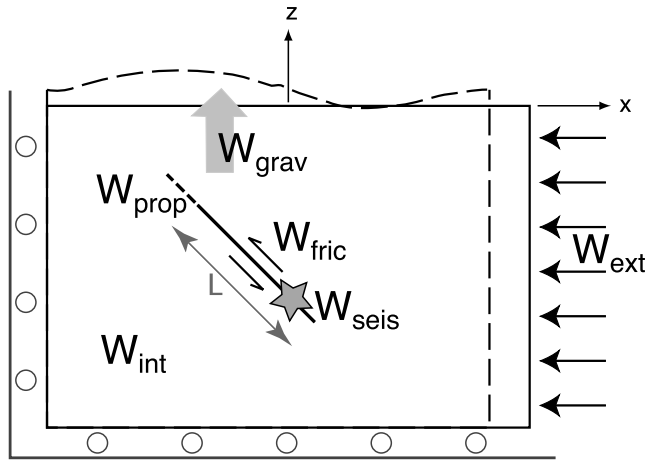

Figure 1. Conceptualization of work components within an idealized single-fault system under horizontal contraction. The left and bottom boundaries are allowed to slide but do not permit normal displacement. The dashed lines represent the shape of the conceptual model boundaries and fault after deformation and propagation. The work of internal strain (W_{int}) work against gravity (W_{grav} and large gray arrow) work against friction along the fault (W_{fric} and small arrows) work of fault propagation (W_{prop}), work of seismic energy released (W_{seis} and star) and external work (W_{ext} and horizontal arrows) are shown schematically.

fault. Fourth, where fault slip takes the form of earthquake events, seismic energy is lost from the system in the form of ground motion (W_{seis}). Finally, work is done in initializing new faults and propagating existing faults (W_{prop}). This work depends on the amount of new fracture surface area produced. The energy budget of the system can thus be expressed as:

$$W_{TOT} = W_{fric} + W_{int} + W_{grav} + W_{seis} + W_{prop}, \qquad (1)$$

where W_{TOT} is the total energy consumed during deformation.

[8] We consider each of these components in turn, using a simple two-dimensional single fault for illustration (Figure 1). Each of these work terms is first formulated in three dimensions and then simplified to two dimensions for application to the numerical models of this study. The two dimensional analysis demonstrates the effectiveness of this methodology for analyzing fault systems and can be extended to three dimensions when the appropriate Boundary Element Method (BEM) tools are available.

2.1. Work Against Gravity

[9] Regional contractional strain results in a net increase in elevation of the region. Although localities within a contracting mountain belt may experience local extension and associated downdrop, the overall vertical movement of the deforming region is upward. This requires that work be done against gravity. Conversely, in extensional regimes, the overall work against gravity is negative, indicating that

work is being done by gravity; that is, gravity contributes to the extensional deformation.

[10] Even in the absence of faulting, horizontal contraction produces increased elevation through vertical dilation of rock material, expressed by the material's Poisson's ratio. In addition, slip on faults under horizontal contraction results in movement of the hanging wall up the fault ramp against the force of gravity. There may also be downward movement of the footwall, but the hanging wall generally has greater upward displacement than the footwall downward because the shallower material has less overburden to resist deformation. Although not considered explicitly in this study, in extension overall elevation decreases as the hanging wall moves down the footwall. A complete calculation of work done by gravity must account for all of these effects.

[11] We calculate all work against gravity by considering the change in gravitational potential energy between the initial, undeformed state and the final deformed state. Because gravitational work is conservative and not path-dependent, we need consider only the final deformation state. This is not the case for all of the work components. The change in gravitational potential energy at a point, ΔU_g, is

$$W_g = \Delta U_g = m\,g\,d_z \tag{2}$$

where m is the mass being displaced, g is the gravitational constant, and d_z is the vertical displacement of the point [e.g., *Young and Freedman*, 1996].

[12] In a deforming region, the vertical displacement will vary with both horizontal position and with depth, z. The mass displaced by the vertical displacement varies with depth based on the density, ρ, so that a column with length dx and width dy will have a mass $\rho\ z\ dx\ dy$. The total gravitational work is then

$$W_{\text{grav}} = \iiint \rho g d_z(z) dz\ dx\ dy, \tag{3}$$

where x and y give the horizontal position and z the depth of the point in the undeformed state. We use ρ, x, y, and z from the undeformed state because the mass of the column of rock, $\rho\ z\ dx\ dy$, remains constant although both the shape of the column and density change in response to contraction; that is

$$\rho\ z\ dx\ dy = \rho'\ z'\ dx'\ dy', \tag{4}$$

where the superscript indicates the deformed state. In the two-dimensional case we consider a cross-section of unit width, so that equation (3) becomes

$$W_{\text{grav}} = \iint \rho g \mathrm{d}_z(z) dz dx. \tag{5}$$

2.2. Work Done in Internal Strain of the Host Rock

[13] Tectonic stresses also perform work in the form of internal strain within the rock surrounding the fault, referred to as the internal strain energy of the rock [*Timoshenko and Goodier*, 1934]. *Timoshenko and Goodier* [1934] derive a general formula for internal strain energy, based on summing the work done by the local stress and strain for an infinitely small increment of strain. For example, in the horizontal x direction

$$dW_{xx} = \sigma_{xx}\ dy\ dz\ \varepsilon_{xx}\ dx, \tag{6}$$

where σ_{xx} is the horizontal stress in the x direction, $dy\ dz$ is the area over which the stress acts, ε_{xx} is the strain in the x direction, and dx is the length subject to the strain. In contrast to the gravitational term, the stresses vary with strain, so that the incremental work calculated above must be integrated over the entire strain. This integral can be simplified if we assume that the rock behaves linearly-elastically, which is realistic for infinitesimal strains (under 1%) such as characteristic of earthquake recurrence timescales. Then,

$$\int \sigma_{ij}\varepsilon_{ij} = \frac{1}{2}\sigma_{ij}\varepsilon_{ij}. \tag{7}$$

This is in contrast to frictional work and external work; for those terms stress depends on strain but is not linear so that the integral cannot be simplified. Summing over all six components of stress gives a total work of

$$dW = V_0\,dx\ dy\ dz, \tag{8a}$$

where

$$V_0 = 1/2\left(\sigma_{xx}\varepsilon_{xx} + \sigma_{yy}\varepsilon_{yy} + \sigma_{zz}\varepsilon_{zz} + 2\sigma_{xy}\varepsilon_{xy} + 2\sigma_{yz}\varepsilon_{yz} + 2\sigma_{xz}\varepsilon_{xz}\right). \tag{8b}$$

V_0 is the amount of work per unit volume, or strain energy density [*Timoshenko and Goodier*, 1934].

[14] Strain energy density (SED) measures the elastic strain energy stored at any point within the host rock. We expect that SED will vary systematically in response to slip on faults. SED shadows may develop adjacent to slipping faults where the strain within the rock has lessened and SED may concentrate in locally deformed areas, such as around fault tips. SED analysis has been applied to evaluate shear fracture propagation in en echelon fault arrays [*Du and Aydin*, 1993] and to evaluate the mechanical efficiency of alternative fault interpretations [*Cooke and Kameda*, 2002; *Griffith and Cooke*, 2004].

[15] The plane strain conditions for our two-dimensional fault system ($\varepsilon_{yy} = \varepsilon_{xy} = \varepsilon_{yz} = 0$) reduce the expression to only three terms. To further simplify the strain energy expression, we can apply the elastic constitutive equations to express V_0 in terms of only stress and elastic properties E (Young's modulus) and ν (Poisson's ratio).

$$V_0 = \frac{(1-\nu^2)}{2E}\left(\sigma_{xx}^2 + \sigma_{zz}^2\right) + \frac{(1+\nu)}{E}\left(\sigma_{xz}^2 + \nu\sigma_{xx}\sigma_{zz}\right). \tag{9}$$

[16] In examining the work budget of an entire fault system, we are concerned with the total work consumed in the form of internal strain energy, W_{int}. Because SED

varies across a faulted area, the total work W_{int} is calculated by summing over the entire area

$$W_{\text{int}} = \int\int V_0(x,z)dxdz. \tag{10}$$

2.3. Work Against Friction

[17] When a fault slips in response to a tectonic strain, work is done resisting friction along the fault surface. The frictional resistance stress, τ_{fric}, is a component of the shear stress along the fault and equals the fault's friction coefficient, μ, multiplied by stress normal to the fault, σ_N, for any compressive normal stress ($\sigma_N < 0$); for a zero or tensile normal stress, τ_{fric} always equals 0. The total shear stress along the fault includes any shear stress induced by gravity, which is accounted for in W_{grav}. For any one segment of the fault with area dA the frictional work, W_{fric}, is generalized as

$$W_{\text{fric}} = -\sigma_N \mu s dA, \quad \sigma_N < 0, \tag{11a}$$

$$W_{\text{fric}} = 0, \quad \sigma_N \geq 0, \tag{11b}$$

where σ_N is the normal stress across the fault, dA is the area of the fault segment, μ is the friction coefficient, and s is slip. For freely slipping faults, $\mu = 0$ and no work is done against friction. Both σ_N and s may vary along the length of the fault. Work done along the whole two-dimensional fault of length l (Figure 1) during an increment of slip can be expressed as

$$W_{\text{fric}} = \int_0^L \sigma_N(l)\mu s(l)dl. \tag{12}$$

In addition, the normal stress and slip will vary as the tectonic strain varies, and as increased topography over the fault increases lithostatic compression. Consequently, σ_N and s depend on the horizontal tectonic strain ε_{hor} and the complete work term in two dimensions,

$$W_{\text{fric}} = \int\int \sigma_N(\varepsilon_{\text{hor}}, l)\mu s(\varepsilon_{\text{hor}}, l)d\varepsilon_{\text{hor}}dl, \tag{13}$$

incorporates both an integration along the fault length as well as an integration along tectonic loading path. In contrast to the nonstrain path-dependent treatment of the internal strain energy term, W_{int}, we must consider the strain integral in calculation of W_{fric} because the dependency of σ_N and s on the tectonic strain is not linear. Although the material may be assumed linear elastic, the presence of frictional faults supplies nonlinearity to the system. The frictional work is also nonconservative; work done resisting friction is converted to heat and absorbed by the surrounding rock. Heat flux measured near the earth's surface can be used to assess the frictional resistance of active faults [*Scholz*, 2002].

2.4. Seismic Energy

[18] In addition to the work that is expressed as observable deformation, energy may be consumed in an actively deforming region through seismic energy lost to the environment in the form of ground motion during earthquake events, W_{seis}. This term is related to the seismic moment. The seismic energy released for a two-dimensional fault of length l is

$$W_{\text{seis}} = \int\int \Delta\tau(\varepsilon_{\text{hor}}, l)s(\varepsilon_{\text{hor}}, l)\, d\varepsilon_{\text{hor}}dl, \tag{14}$$

where $\Delta\tau$ is the change in shear stress associated with fault slip and s is slip [e.g., *Scholz*, 2002]. Once again slip, as well as shear stress drop, depends on the tectonic strain, ε_{hor}, so that seismic work must be integrated over the loading path.

[19] If faults are permitted to slip wherever the shear stress exceeds a constant frictional resistance (σ_N μ), slip occurs without earthquake events, and the fault creeps. In that case, the shear stress is maintained at the level of frictional resistance, so that there is no shear stress drop, and W_{seis} equals zero. Seismic energy of earthquakes is associated with stick slip, where the friction coefficient on the fault surface is reduced as the fault slips. Rate and state friction theory demonstrates the release of seismic energy with drop of friction coefficient from static to dynamic levels [e.g., *Marone*, 1998]. The opposing end-member to a creeping fault is a fault that releases all of its accumulated shear stress within one earthquake event. The seismic energy calculated along such a fault represents the maximum possible energy released over the time considered.

2.5. Work Initializing and Propagating Faults

[20] The work done in initializing new faults and propagating existing faults, W_{prop}, can be calculated using the surface energy of a crack, γ, the energy per unit area required to break the bonds of the material [e.g., *Scholz*, 2002; *Lawn and Wilshaw*, 1975]. Experimental studies have shown that the critical surface energy values for fault propagation depend on normal compression and range from 10^1 to 10^4 J m^{-2} [*Wong*, 1982, 1986; *Cox and Scholz*, 1988]. These experiments consider the surface area created by microcracking adjacent to sliding fault surfaces. W_{prop} for the fault system depends on the total surface area created during fault growth; this includes not only the primary fault surface and associated microcracks but also the surface areas within a zone of cataclasite along the fault [*Scholz*, 2002; *Mitra and Boyer*, 1986]. This cataclastic zone includes macroscale faults. The complete relationship can be expressed as

$$W_{\text{prop}} = \gamma p + \gamma pwr, \tag{15}$$

where γ is the surface energy per unit length, p is the added length of the fault, w is the width of the cataclasite zone, and r is the density of secondary faults in the zone [*Mitra and Boyer*, 1986].

2.6. Total Work and External Work on the System

[21] The total work done within the system is the sum of all five of the components discussed above. A summary of the formula of the work components in two dimensions is set forth in Table 1.

Table 1. Formula for Each Work Component in Two Dimensions

Work Component	Symbol	Characteristics	Two-Dimensional Formulation
Work against gravity	W_{grav}	conservative, nonpath-dependent	$\int\int \rho g d_z(z) dz dx$
Internal strain energy	W_{int}	conservative, linear-elastic, nonpath-dependent	$\int\int V_o(x, z) dz dx$
Work against friction	W_{fric}	nonconservative, nonlinear, path-dependent	$\int\int \sigma_N(\varepsilon_{hor}, l)\mu s(\varepsilon_{hor}, l) d\varepsilon_{hor} dl$
Seismic energy	W_{seis}	nonconservative, nonlinear, path-dependent	$\int\int \Delta\tau(\varepsilon_{hor}, l) s(\varepsilon_{hor}, l) d\varepsilon_{hor} dl$
Work creating new fault surface	W_{prop}	nonconservative, nonpath-dependent	$\gamma p + \gamma p w r$
External work	W_{ext}	nonconservative, nonlinear, and path-dependent	$\int\int \sigma_{hor}(\varepsilon_{hor}, z) A \varepsilon_{xx}(z) d\varepsilon_{hor} dz$

[22] Finally, if the far field tectonic stress or strain can be well defined along an appropriate boundary of the system, the total work done in the system, W_{TOT}, equals the work done on the external boundary of the system, W_{ext}, under the principle that work done on the boundary of a closed system equals the increase in energy within the system [e.g., *Young and Freedman*, 1996]. Within geological systems, such boundaries may be plate margin boundaries or zones where strain rates are known from geodesy. Again using our simple application of a constant horizontal tectonic strain, ε_{hor}, the stress, σ_{hor}, along the boundary depends on this tectonic strain as well as depth, z. The complete work term in two dimensions is

$$W_{ext} = \int\int \sigma_{hor}(\varepsilon_{hor}, z) A \varepsilon_{xx}(z)\, d\varepsilon_{hor} dz, \tag{16}$$

where A is the area of the external boundary (boundary height in two dimensions). As with W_{fric}, the nonlinearity of the slipping fault system necessitates consideration of the strain path integral, since the dependence of stress on degree of strain is not linear. Requiring that external work equal the sum of the work components outlined above provides an important check on a complete work balance equation, and provides a single measure with which to assess the total work expended in the deformation of a region.

3. Evaluating Fault System Work Components Using Mechanical Modeling Tools

[23] The work components outlined above can be calculated for a variety of fault systems using analytical or numerical mechanical models. Numerical methods such as finite element method (FEM) and boundary element method (BEM) can simulate deformation associated with complex fault configurations by calculating stress and strain throughout a body due to prescribed tractions or displacements on the model boundaries, using the principles of continuum mechanics [e.g., *Crouch and Starfield*, 1990]. All the data necessary for the analysis, including slip, traction, internal stress and stain and vertical displacements, are constrained by the governing differential equations of continuum mechanics. A comparison of numerical results to analytical solutions for simple situations provides a means of assessing the error of numerical results.

[24] This study utilizes BEM models. Unlike FEM, which requires discretization of the entire body, BEM only requires discretization of model boundaries and discontinuities (i.e., faults). This is advantageous for modeling multiple interacting faults because BEM requires less effort for discretization, and errors due to discretization and approximation arise only on the boundaries and along fault surfaces [*Crouch and Starfield*, 1990].

[25] This study employs a two-dimensional BEM code, FRIC2D, that computes elastic and inelastic deformation associated with frictional slip along faults using the displacement discontinuity formulation of *Crouch and Starfield* [1990] with special constitutive frictional slip elements [*Cooke and Pollard*, 1997]. The model boundaries and fault are discretized into linear elements each with uniform shear and normal displacement discontinuities. The models are finite and the position and orientation of the model boundaries can be prescribed to simulate a wide range of conditions. For example, nonrectangular boundaries have been used to simulate deformation over buried craters on Mars [*Buczkowski and Cooke*, 2004]. Additionally, fault geometry is prescribed by the positions and orientations of the fault elements. FRIC2D requires prescription of the faults' constitutive properties (i.e., frictional strength) [*Cooke and Pollard*, 1997]. FRIC2D has been used to investigate the early stages of fault-related fold development [*Cooke and Pollard*, 1997], bedding plane slip within folds [*Cooke et al.*, 2000], joint propagation near bedding planes [*Cooke and Underwood*, 2001], and blind thrust fault propagation [*Roering et al.*, 1997].

[26] FRIC2D incorporates idealizations that do not reflect all geological conditions. The models assume a linear elastic rheology that omits time-dependent viscoelastic effects that may be important on long timescales [e.g., *Rundle*, 1982; *Cohen*, 1984]. The models also assume homogeneous and isotropic material properties, a potentially major simplification depending on the rock types in the area of concern. This technique therefore captures only the first-order effects of fault configuration on work; differences due to rock rheology must be assessed independently.

3.1. Model Setup

[27] To illustrate this analysis, we again consider the case of a single fault under contraction, as modeled using the BEM code FRIC2D (Figures 1 and 2). The rock surrounding the fault is homogeneous, linear elastic and isotropic. The material properties used were chosen based on the rock types in the Los Angeles basin for consistency with models presented in section 8; these values represent an average over a range of sedimentary, metamorphic and igneous rock types [*Cooke and Kameda*, 2002] A uniform leftward displacement is applied to the right hand boundary of the model to produce 1% contractional strain across the model. A bilateral gravitational stress field is superposed on the model with

$$\sigma_{zz} = \rho g z \tag{17a}$$

$$\sigma_{xx} = \frac{\nu}{1-\nu} \rho g z, \tag{17b}$$

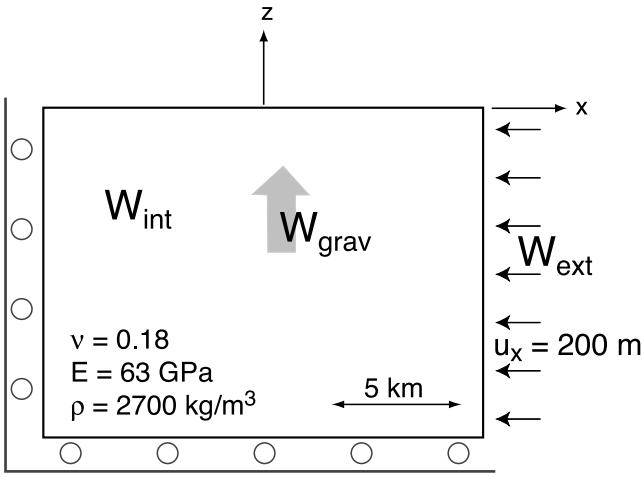

Figure 2. Configuration of the faultless model used to compare the boundary element method results with the analytical solution. Material properties, Poisson's ratio, ν, Young's modulus, E, and density, ρ, are shown. The model is contracted by displacement of the right boundary 200 m to the left. The only nonzero work terms are external work, W_{ext}, internal work, W_{int}, and work against gravity, W_{grav}.

where ρ is density, g is gravitational acceleration, ν is Poisson's ratio, x is horizontal position and z is elevation (negative below the surface); compressional stress is negative. The nonuniform σ_{xx} prevents heterogeneous lateral expansion of the model that results from lithostatic ($\sigma_{xx} = \sigma_{zz} = \rho g z$) stress state [e.g., *Engelder*, 1993; *Jaeger and Cook*, 1976]. For the first few sets of models (sections 4 and 5), the system is static; the fault is not permitted to propagate and no additional faults may initiate (i.e., $W_{prop} = 0$). In addition, the fault slips whenever the shear stress on the fault exceeds the frictional resistance, and does not experience earthquake events (i.e., $W_{seis} = 0$). This analysis does however provide implications for W_{seis}, discussed later in this paper (sections 6, 8, and 9).

[28] The inelastic nature of the fault system results in the loading path dependencies of several work terms (e.g., W_{fric} and W_{ext}). To minimize this path dependency, the models are loaded in small monotonic steps to the prescribed final condition. At each loading step, the inelastic frictional slip along the faults requires iterative solution until the system converges [*Cooke and Pollard*, 1997]. A user prescribed tolerance is used to assess convergence.

3.2. Validation of Numerical Results by Comparison to Analytical Solution

[29] For validation purposes, we first consider the work budget of an unfaulted block (Figure 2). Because there are no faults, $W_{fric} = W_{prop} = W_{seis} = 0$, and the entire energy balance equation simplifies to

$$W_{int} + W_{grav} = W_{TOT}; \tag{18a}$$

for energy balanced system,

$$W_{TOT} = W_{ext}. \tag{18b}$$

The external work applied along the boundary is partitioned into internal strain energy and uplift against gravity (Table 2). The numerical model total of W_{int} and W_{grav} is within 0.01% of the external work computed along the boundary, adequately simulating energy-balanced deformation in the unfaulted case. To assess the error of the numerical method we compare the results with analytical solutions for deformation in the deformed block. This comparison illustrates that the W_{grav} term incurs the greatest error of <2%. This small error is likely due to sampling and/or discretization effects. We encounter sampling errors because we calculate internal strain energy and gravity by summing over a grid of observation points; the error was reduced by increasing the density of the grid and would be zero for an infinitely dense grid. Discretization effects are due to the treatment of boundary and fault surfaces as a series of elements with uniform displacements and stresses; this error was reduced by reducing the element size (increasing the number of elements). The latter error is likely to increase with consideration of faults in the model, as the amount of discretized area (boundaries plus faults) increases. The error of the faulted models can be assessed indirectly by summing the work terms and comparing to external work; these are reported within subsequent sections. We consider errors within a few percent of the work to be suitably small for this study, thus requiring no further refinement of the model.

4. Static One-Fault System

[30] We next consider 6 km long frictional and frictionless faults dipping 35° (Figure 3). For these static models, the faults are not permitted to propagate (i.e., $W_{prop} = 0$) and do not experience stick slip resulting in earthquake events, so $W_{seis} = 0$. To minimize the path-dependent effects of the frictional and external work, these models are loaded monotonically in four steps. The model results are set forth in Table 3.

[31] For the frictionless case, the total of W_{int} and W_{grav} is within 0.1% of the external boundary work; the faulted model is less balanced than in the no fault case. This is likely due to the additional discretization effect along the fault leading to uncertainty in accounting for the internal strain at points near the fault that the BEM cannot reliably calculate. Discretization of the fault into a greater number of smaller elements will reduce this discrepancy; however we consider these errors to be suitably negligible. Addition of the freely slipping fault results in a reduction in the internal strain energy from the no fault case, and an offsetting increase in gravitational work. Adding a fault reduces the internal strain, but at a "cost" of increased work against gravity. The reduction in strain energy is greater than the corresponding increase in the other work terms, so that less total work is required to deform a faulted area than an

Table 2. Work Balance for Faultless Case, Comparing Numerical Model and Analytical Results[a]

	W_{int} +	W_{grav} =	W_{TOT}	W_{ext}
Numerical	976.4	128.8	1104.8	1105.3
Analytical	976.6	130.8	1107.4	1107.4
Error	−0.2	−2.0	−2.2	−2.1

[a] W_{int} and W_{grav} are the only nonzero work components. Work values are in terajoules.

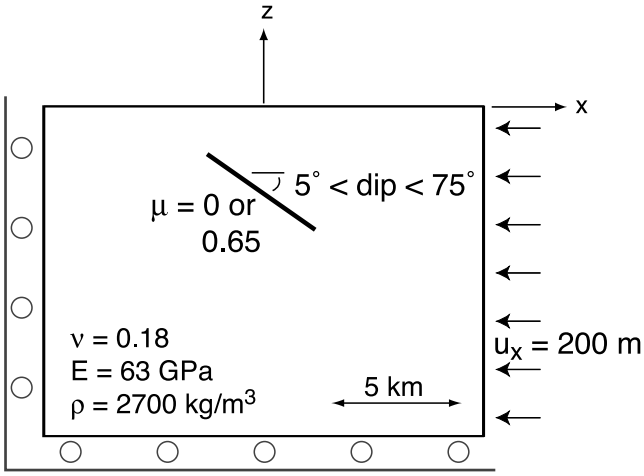

Figure 3. Configuration of single-fault model. The friction coefficient along a 35° dipping fault assigned either 0 or 0.65 in order to assess the sensitivity of the work balance to presence of work against friction. In another set of numerical experiments, fault dip varies from 5° to 75° to explore the sensitivity of fault dip on the distribution of work.

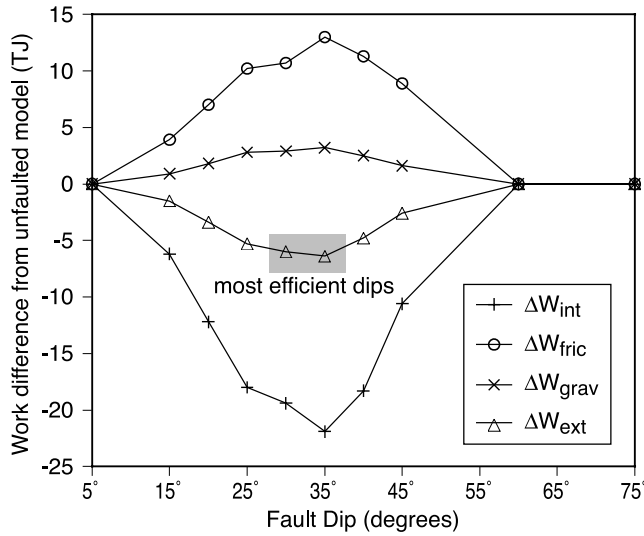

Figure 4. Difference for all work components between the faulted and unfaulted models under varying fault dips and 0.65 friction coefficient. Faults with very shallow (dip $\leq 5°$) or steep (dip $\geq 60°$) dips do not slip under the modeled horizontal contraction modeled. The 30°–35° dipping faults have the lowest external (W_{ext}) work and are the most efficient fault dips to accommodate horizontal contraction. The 35° fault has lesser internal work (W_{int}) and greater work against gravity (W_{grav}) than the 30° dipping fault. The most efficient fault dips found here by work minimization fall within the range of faulting observations in triaxial tests (20°–40° [*Handin*, 1966; *Goodman*, 1989]).

unfaulted one. Taken to the extreme, we might then expect a dense spiderweb-like network of faults to develop in order minimize energy; however, the production of fault surface area consumes energy. Many small faults have greater surface area and require greater W_{prop} than a few longer faults. The energy required for fault propagation is explicitly considered in section 9.

[32] We then consider the same fault with a constant friction coefficient of 0.65, within the range of friction coefficients found in laboratory sliding experiments [*Byerlee*, 1978]. The numerical model continues to produce a reasonably close energy-balanced budget (within 0.1%, Table 3). The imbalance is similar to that for the frictionless fault. As expected, the frictional fault work results lie between the end-members of freely slipping and no fault models. The frictional fault case requires more energy to produce the prescribed strain than the frictionless fault, but less energy than the no fault case. The frictional fault produces a reduction in W_{int} from the no-fault case with offsetting increases in both W_{grav} and W_{fric}.

5. Frictional Faults at Varying Dips

[33] Next, we consider a 6 km frictional fault at varying dips. Once again loading is applied over 4 steps and the faults are static. For this analysis, we are concerned with the relative changes in each work term; accordingly, Figure 4 shows the difference in work components from the unfaulted case. The work terms vary consistently with dip. Addition of any slipping fault reduces the internal strain energy, and produces offsetting increases in frictional and gravitational work. Once again, the reduction in strain energy exceeds the corresponding increase in the other work terms, so that less total work is required to deform faulted regions than unfaulted ones. However, unfavorably oriented faults, i.e., faults that do not slip, do not reduce the total work.

Table 3. Work Balance for 35° Dipping Fault Model[a]

	W_{int} +	W_{grav} +	W_{fric} =	W_{TOT}	W_{ext}
No fault	976.4	128.8	0.0	1105.2	1105.3
Frictionless fault	934.2	138.3	0.0	1072.5	1071.9
Frictional fault	954.5	132.0	13.0	1099.5	1098.9

[a]Frictionless and frictional ($\mu = 0.65$) faults are compared to faultless case. The system is static, with no earthquake events and no fault propagation, so that W_{seis} and W_{prop} are zero. Work values are in terajoules.

[34] The premise of work minimization leads us to expect that the faults most likely to develop within an evolving system would be those requiring the least work to accommodate the same tectonic strain. Our model shows that faults dipping 30°–35° require the least external work. The 35° dipping fault has lesser internal work than the 30° dipping fault, but this work benefit is tempered by the greater work expended against gravity for the 35° dipping fault. These fault dips are within the range of failure surface orientations observed in triaxial tests [e.g., *Handin*, 1966; *Goodman*, 1989]. Furthermore, the most efficient fault dips may depend on friction coefficient. For example, freely slipping faults are expected to provide the greatest energy savings at 45° dip, the plane of maximum shear stress under horizontal contraction.

6. Consideration of Seismic Energy Release

[35] The work budgets in section 5 describe faults that do not experience earthquake events; these creeping faults

radiate no seismic energy because the faults are constantly responding to the resolved stress state. Although the BEM model does not explicitly include earthquake events, we can calculate the seismic energy that would be released if, for each tectonic loading step, the slip on all faults within the model occurred in a single earthquake event. To do this, we compare the total work required to strain the faultless model, equivalent to a locked fault, to the external work required for the faulted model. The change in energy, ΔW_{ext}, reflects the seismic work released due to the fault slip.

[36] Alternatively, the seismic energy released can be calculated directly using equation (14) by integrating over the tectonic loading the fault slip and associated change in shear stress. For each loading step, we calculate the change in slip from the previous step and the drop in shear stress before and after slip. As with the ΔW_{ext} method, all faults are assumed to slip in one earthquake during each loading step and the shear stress drop is assumed to occur linearly throughout the modeled slip (Figure 5a).

[37] In order to assess the accuracy of the two methods, we compare the change in external work to the direct calculation of seismic work for a 35° dipping frictionless fault (Table 4). For this case, ΔW_{ext} is within several terajoules of the calculated W_{seis}. This difference is similar to the error of the numerical calculations of W_{ext} (Table 2) so that either method can be used to calculate seismic energy released. For these creeping faults, we prefer calculating ΔW_{ext} because of the ease of computation.

[38] The calculations of seismic energy from the fault models represent a maximum potential release of seismic energy because dynamic stress drops during slip are not considered. The calculations of seismic energy assume that the shear stress drop associated with the earthquake occurs linearly throughout the slip of the earthquake event (Figure 5a). However, laboratory studies have shown that dynamic stress drops are focused at the onset of slip [e.g., *Dieterich*, 1979] (Figure 5b). If the shear stress drop occurs over a smaller slip, lesser seismic energy is released even though the total work of the system is unchanged. The ratio of seismic energy released in earthquakes and laboratory slip events to the energy available has been expressed as seismic efficiency, η [e.g., *McGarr*, 1999]. Within this study, we have neglected dynamic stress drops so that $\eta = 1$ and the seismic energy released equals the change in total work ($W_{seis} = \Delta W_{ext}$). However, earthquakes and laboratory slip events have been shown to have seismic efficiencies smaller than 0.06 [*McGarr*, 1994, 1999]. We should note that here we calculate the change in total work of the system as the available energy, whereas *McGarr* [1999] uses the change in internal energy (W_{int}). These formulations are identical if work against gravity (W_{grav}) and frictional heating (W_{fric}) are assumed to be negligible.

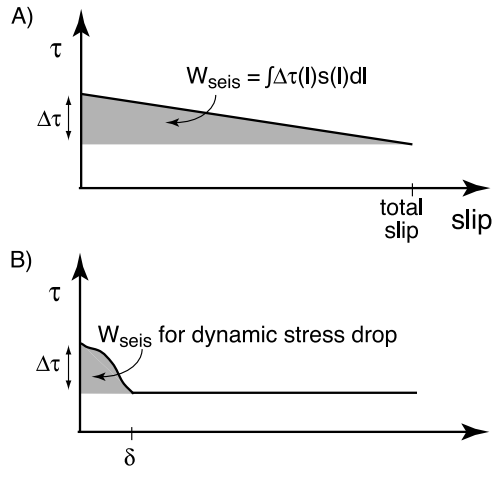

Figure 5. Comparison of seismic energy release from (a) one tectonic loading step within the loading path integral of equation (14) and (b) one slip event (earthquake) with dynamic shear stress drop. The seismic energy released is the grey area under the τ slip curve. The δ represents the critical slip distance over which the friction evolves to steady state.

Table 4. Seismic Energy Released for a Frictionless 35° Dipping Fault[a]

	W_{ext}, TJ	ΔW_{ext}, TJ	Calculated Seismic Energy, TJ
No fault	1105.3		
Frictionless	1071.9	33.4	36.4

[a]Calculated seismic energy (equation (14)) is compared to change in external energy between preearthquake (locked or no fault) and postearthquake (frictionless) cases.

7. Consideration of Fault Propagation

[39] In order to explore the final component of the work budget, W_{prop}, and its implications for studying fault system evolution, we consider the propagation of a fault in our simple one fault system. Starting with our single 6 km long fault dipping 35° we propagate the fault in two directions in alternative models. The first extends the original fault 1 km toward the surface, maintaining a dip of 35°. The second propagates as a 1 km long back thrust, initiating at the midpoint of the original fault, and dipping 35° in the opposite direction (Figure 6).

[40] As expected, the extension of the original fault reduces the total work required to produce the prescribed displacement on the boundary (Figure 6b). As with the previous models, addition of the slipping fault surface reduces W_{int} and increases W_{grav} and W_{fric}, with a lower total work, W_{ext}.

[41] In contrast, addition of a back thrust does not reduce the total work. A small degree of reverse slip on the back thrust reduces W_{int} but also increases work against friction (W_{fric}) and work against gravity (W_{grav}) relative to the original fault system. Using our criteria that we would only expect fault growth that decreases the total work of the system, we would expect extension of the original fault rather than development of a back thrust under our model conditions. Other studies suggest that back thrusts may only be favored in conditions with interlayer slip [*Nino et al.*, 1998] or under specific conditions of topography and erosion [*Masek and Duncan*, 1998].

[42] While extension of the original fault reduces total work in the static energy balance, the cost of this fault propagation is not accounted for in that balance: Energy is required to break the rock and create new fault surface (W_{prop}). The overall efficiency of the system is only

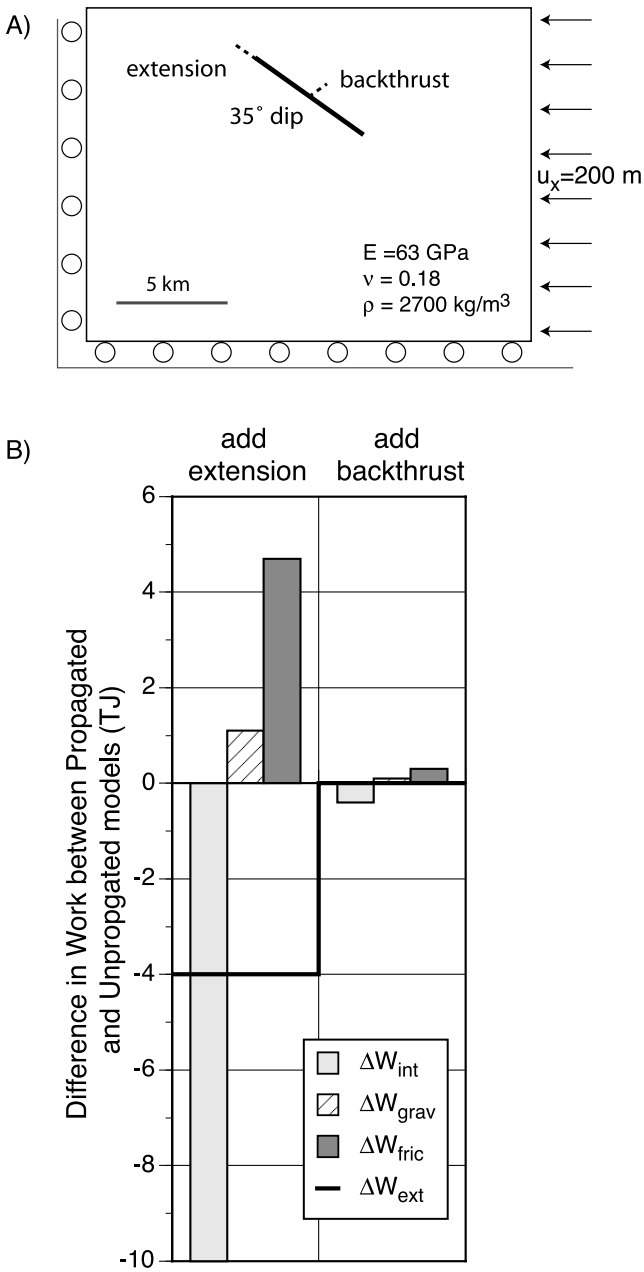

Figure 6. (a) Alternative propagation paths of a 35° dipping two-dimensional fault include (1) extension within the plane of the fault or (2) development of a back thrust. (b) Propagation by extension of the fault provides a greater energy savings than propagation by back thrusting. The systemic energy savings of 4 TJ achieved by extending the fault exceeds laboratory estimates of the energy required to create the new fault surface, W_{prop}.

increased if the energy saved by extension of the fault exceeds the energy required to create the fault.

[43] Following *Mitra and Boyer* [1986], we use the relationship of (15) to estimate W_{prop}. Experimental studies have shown that the critical surface energy values, γ, for various rock types, depend on normal compression and range from 10^1 to 10^4 J m^{-2} [*Wong*, 1982, 1986; *Cox and Scholz*, 1988]. Because mode III fault propagation generally shows γ at the lower end of this range 10^1–10^2 J m^{-2} [*Cox and Scholz*, 1988], a higher surface energy should be considered for the mode II propagation simulated in this study. The thickness of the granulated fault zones has been estimated as 1/10 to 1/100 the fault displacement [*Robertson*, 1983; *Scholz*, 1987]. *Mitra and Boyer* [1986] use 500 m^{-1} for the density of secondary faults in the cataclastic zone.

[44] Substituting these values into (15) for added fault length of 1 km with maximum displacement of 23 m, gives a W_{prop} of ~1–11 GJ. Even though this analysis includes consideration of a cataclastic fault zone, the energy required to propagate the fault is several orders of magnitude smaller than the change in efficiency (Figure 6), which is on the order of Terajoules. Thus the fault propagation energy is insignificant compared to the other forms of work energy, consistent with the findings of *Mitra and Boyer* [1986] and the analytical calculations of *Scholz* [2002]. This indicates that for the tectonic contraction modeled here, growth of a fault extension of this length would easily be favored under efficiency criteria.

8. Application of Two-Dimensional Work Budget to the Los Angeles Basin

[45] The final application of the work balance method considers a transect across the Los Angeles Basin. The Los Angeles Basin is undergoing active crustal deformation expressed as slip along a three-dimensional system of interacting faults [e.g., *Yerkes*, 1965; *Davis et al.*, 1989; *Wright*, 1991; *Shaw and Suppe*, 1996; *Shen et al.*, 1996; *Walls et al.*, 1998]. Sets of active NW trending faults (including the Whittier, Newport-Inglewood and Palos Verdes faults) and E–W trending faults (including the Malibu-Santa Monica-Raymond Hill fault system) are believed to interact via a subsurface system of horizontal detachments and thrust ramps at ~10–15 km depth [*Davis et al.*, 1989; *Shaw and Suppe*, 1996].

[46] We consider a two-dimensional model of faults in the Los Angles basin along a cross section from the Palos Verdes Hills to the Whittier Hills (Figure 7a). The subsurface fault geometry (Figure 7b) is based on kinematic inferences from overlying fault shape [*Shaw and Suppe*, 1996]. A 0.5% contraction, applied by translating the right side of the model, represents ~50,000 years of contraction at current strain rates [e.g., *Argus et al.*, 1999; *Bawden et al.*, 2001]. We consider two models, one with frictionless faults and a second with faults having a uniform friction coefficient of 0.4, which simulates mature fault surfaces weakened by fluids and falls within the range of values suggested by previous researchers [*Deng and Sykes*, 1997; *King et al.*, 1994; *Scholz*, 2000; *Cooke and Kameda*, 2002]. To minimize the path-dependent effects of the frictional and external work, these models are loaded monotonically in eight steps. At each step, the model solution is iterated to convergence so that the faults are in equilibrium with their surrounding stress state.

[47] Even with a far more complex network of faults than presented thus far, the work budget is reasonably close to being energy balanced (i.e., $W_{TOT} \sim= W_{ext}$; Figure 8a). The imbalance is 7.3% for the frictionless case and 0.5% for the frictional case.

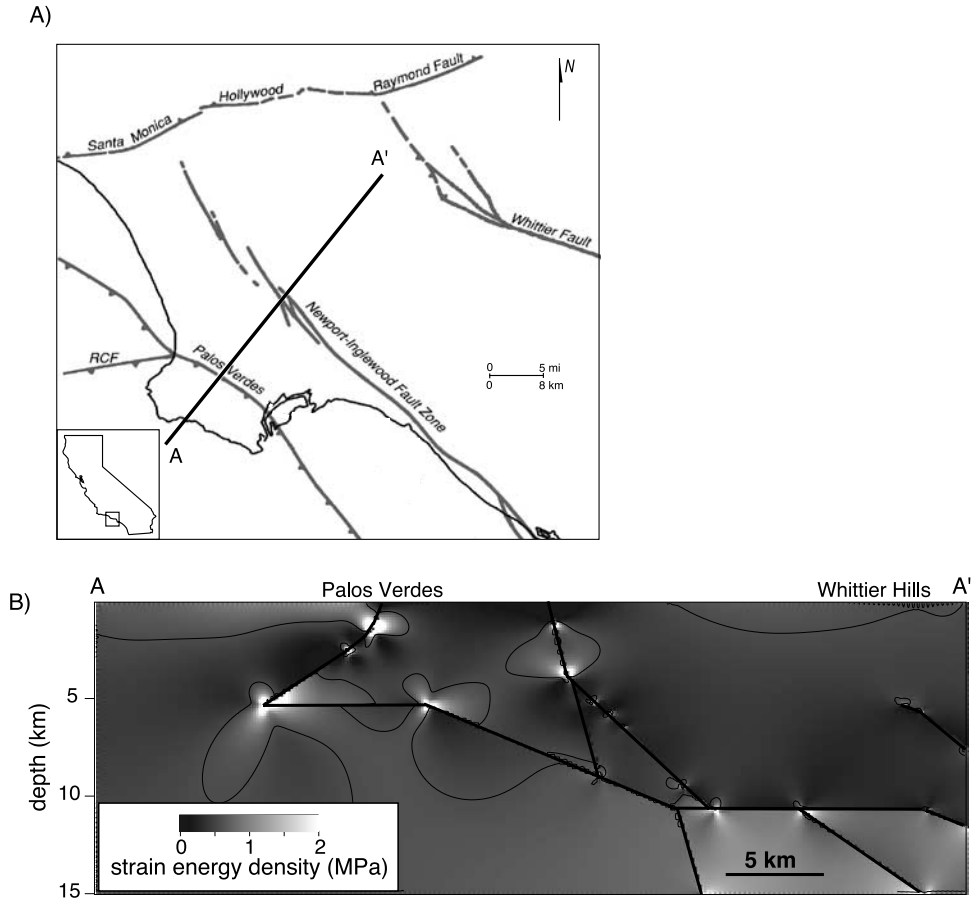

Figure 7. (a) Fault map of the Los Angeles Basin, California. The bold line marks the approximate trace of the cross section studied (modified from *Wright* [1991] and *Cooke and Kameda* [2002]. (b) Fault model showing distribution of internal strain around the freely slipping faults. The average strain energy density for the model (0.58 MPa) is contoured. Bright regions have greater than average internal strain whereas dark areas are in the strain shadows of slipping faults.

[48] As expected, the reduction in total work from an unfaulted case is far greater for a frictionless fault network than for the frictional faults, due to far greater slip occurring on faults when they slip freely (Figure 8b). Although the frictionless faults exhibit greater uplift against gravity, as a consequence of greater fault slip, the drop in W_{int} more than compensates for the increase in work against gravity, W_{grav}. In addition to the greater reduction in W_{int}, faults that slip completely freely require no work against friction to accommodate sliding deformation.

[49] The energy balance continues to be dominated by the internal strain energy. In the frictional faults case, the work expended overcoming frictional resistance is ~2% of the work expended in internal strain energy. This suggests that far less energy may be transferred to heat flow than to uplift and deformation of host rock. However, the proportions of internal work to frictional work and seismic work should be considered in the context of the simplistic two-dimensional deformation of the models. Contraction across the Los Angeles basin is accommodated by strike-slip as well as reverse slip so that three-dimensional models incorporating strike slip may produce greater W_{fric} and lesser W_{int} than two-dimensional models. The partitioning of work components is discussed further in section 9 of this paper.

[50] We can calculate the cumulative seismic energy that would be released if all of the faults slipped within in a single earthquake event per loading step. The following relationship can be used to calculate the equivalent earthquake moment, M_S, from the seismic energy released, W_{seis}, [e.g., *Scholz*, 2002]

$$M_S = 2/3 \log(W_{\text{seis}}) - 3.2. \tag{19}$$

If the faults slipped without frictional resistance in one earthquake event over the modeled time period (50,000 years), 23 TJ of seismic energy would be released equivalent to a M 5.7 earthquake. If the faults slipped frictionally in one earthquake, 6 TJ of seismic energy would be released, equivalent to a M 5.3 earthquake. We can incorporate the reduction in seismic energy expected from dynamic shear stress drop by implementing a seismic efficiency of 0.06 [e.g., *McGarr*, 1999]. The expected earthquake magnitude drops to M 4.9 for the frictionless and to M 4.5 for the frictional cases.

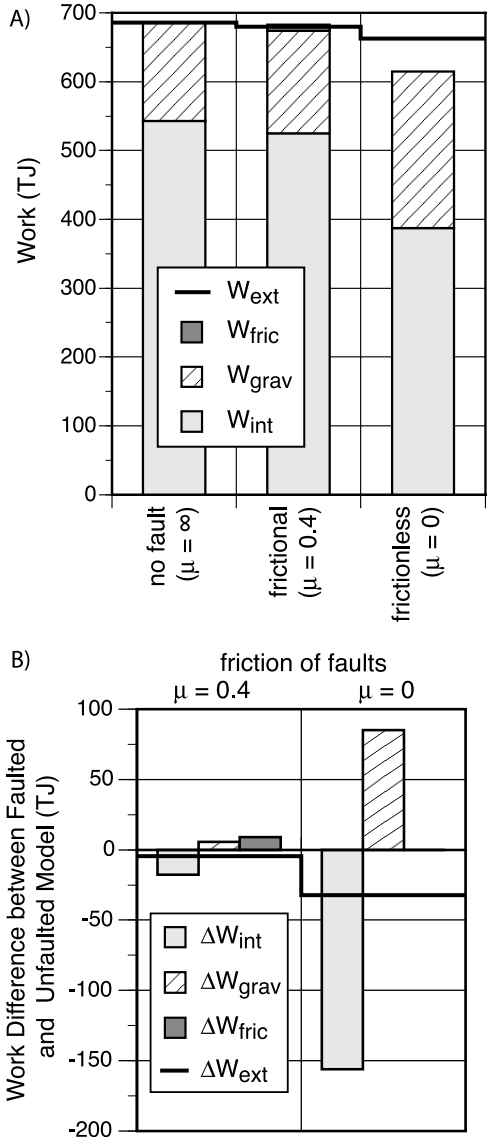

Figure 8. (a) Distribution of work within a two-dimensional system of faults simulating the Los Angeles Basin. Under frictional conditions ($\mu = 0.4$), many faults have limited or negligible slip. Consequently, frictional heating is small and the other work terms resemble results of the unfaulted model. (b) The difference in all work terms between the faulted and unfaulted models. The frictionless fault model is more efficient than the frictional faults despite the added work against gravity, which would be expressed as uplift. The change in external work, ΔW_{ext}, serves as a proxy for seismic energy released if all the faults within the model slipped in one event within 50,000 years. The frictionless faults release greater seismic energy than the frictional faults.

[51] These hypothetical calculations do not reflect accurate earthquake hazards for the region. Because we have modeled only a two-dimensional cross section, we are neither considering the complete three-dimensional slip vector nor considering the complete fault surface area at risk to slipping in earthquake events; consequently, two-dimensional analyses understate the maximum potential for seismic energy release. On the other hand, all of the faults are not expected to release 50,000 years of stored energy within a single earthquake event. Theses calculations overstate the earthquake magnitude expected from events that occur on subsets of the regional faults over recurrence time periods less than 50,000 years.

9. Discussion

[52] A work balance approach to examining fault systems holds great potential for allowing analysis of entire systems of interacting faults and understanding fault system evolution. The numerical models allow us to evaluate the work done on the boundary of a complex system without requiring a detailed analysis of every component of work within the system. This can provide a benefit where the major issue of concern is the overall work required to deform the system, such as in assessing overall fault system efficiency, or providing an overall estimate of seismic energy potential.

9.1. Partitioning of Work

[53] The energy budgets are dominated by internal strain energy, even in the Los Angeles Basin model, a region with substantial faulting. Gravitational work also presents a substantial component of the total work, whereas relatively little energy is expended overcoming frictional resistance.

[54] That is not to say that the influence of frictional work is unimportant, especially when considering the evolution of a system along alternative paths of faulting. While W_{int} is by far the largest work component, the changes in W_{int} among models with differing fault geometries are comparable in magnitude to the changes in W_{grav} and the total frictional work W_{fric} (Figures 4, 6, and 8b). If this were not the case, the work budget would not balance. In our models, then, the path of deformation is being influenced by energy factors that represent a relatively small proportion of the total energy input into the system.

[55] Within natural systems, other processes may contribute to the energy of the system that are not considered here. Chemical reactions such as those that facilitate pressure solution and other inelastic deformation may act to alter the internal work and the external work on the system. Inelastic deformation likely in regions of high internal strain (e.g., bright regions on Figure 7b) may reduce the stress terms in the equations for both W_{int} and W_{ext} and may increase the strain terms within W_{int}. If the stress-strain relations for the inelastic processes are known, they can be considered explicitly within W_{int} (equation (6)) and linear elasticity need not be assumed.

[56] It is possible that the partitioning of work will change as a fault system matures. A fault system in its earliest stages may have a work budget that resembles that of an unfaulted system. In that case, it would be unsurprising that the single-fault models have work budgets dominated by W_{int}. As a matter of efficiency, we expect that a more mature fault system will have a lower total work; we might also expect that the partitioning of work would be different, with less work expressed as W_{int} and more expressed as gravitational work.

[57] We see some evidence for reduction of internal work in our models of extension of the 35° dipping fault, and of the complex Los Angeles fault network. The extension of

the fault reduces total work by reducing W_{int} and increasing W_{grav} and W_{fric}; while both the total work and W_{int} decrease, W_{int} is a smaller proportion of the total work for the extended fault than for the initial fault (86% < 87%). Similarly, in the Los Angeles model the percentage of the work budget consumed in internal strain energy decreases from the unfaulted model (79%) to the frictional fault model (77%) to the frictionless model (58%). The partitioning of work among forms of deformation therefore may be an indicator of the maturity of fault systems.

9.2. Assessing Between Alternative Fault System Configurations

[58] A major focus of previous work analyses has been in determining efficient or minimum work paths of deformation [*Masek and Duncan*, 1998; *Jamison*, 1993; *Dahlen and Barr*, 1989; *Molnar and Lyon-Caen*, 1988; *Mitra and Boyer*, 1986; *Sleep et al.*, 1979]; elements of the work analysis here have been applied for that purpose [*Cooke and Kameda*, 2002; *Griffith and Cooke*, 2004]. The more complete analysis presented here presents evidence in support of these applications. The energy minimization analysis of faults with varying dip found that 30°–35° dipping faults were the most energy efficient, consistent with experimental observations. The energy minimization analysis for alternative fault propagation paths preferred fault extension rather than back thrust development, which has been shown to require heterogeneous conditions.

[59] Although these simple models assume homogeneous rheology, in many regions of the Earth we expect increasing stiffness with depth and/or lateral variations in material properties. Such heterogeneities are expected to locally alter the stress field so that predictions of efficient fault configuration for a homogenous region may not be applicable to heterogeneous region. However, even within regions with heterogeneous material properties, the first-order heterogeneities controlling deformation may be the fault surfaces/zones, which serve to localize deformation.

[60] These results presented in this study demonstrate that the minimum work approach can successfully assess between both alternative fault geometry and/or alternative fault propagation paths. Consequently, these work minimization tools might also be used to predict the propagation and evolution of fault systems.

9.3. Implications for Earthquake Assessments

[61] Our calculations of potential seismic energy release based on creeping faults can provide an upper bound to earthquake seismic moment assessments; the calculations presume 1) that all of the seismic energy in the modeled increment of deformation is released in a single earthquake event and 2) that the shear stress drop occurs throughout the slip event. Although the modeled faults within this study all slip together during each tectonic loading step, earthquakes are generally temporally distributed on individual faults or fault segments. Tectonic loading steps smaller than typical earthquake recurrence intervals (<1000 years) could limit slip events at each step to those fault surfaces that are critically stressed. Alternatively, because earthquakes seem to have a relatively consistent stress drop of ~3 MPa [*Abercrombie*, 1995], we could allow faults to slip whenever the potential shear stress drop exceeds 3 MPa. The second presumption can be accommodated to some degree by using observations of seismic efficiency from earthquakes and laboratory slip events to reduce W_{seis}. Seismic efficiency provides a basis for calculating the apparent seismic energy released from the total energy available [*McGarr*, 1999].

10. Conclusions

[62] The work budget gives a sense of the partitioning of tectonic work among various forms of deformation: frictional heating, uplift, tectonic deformation, fault growth and seismic energy release. The BEM models are shown to produce a balanced work budget for both simple and complex fault system models. Deformation through fault slip permits a region to accommodate tectonic strain with less work done in the form of internal strain of the rock, but at a cost in terms of work resisting friction and increased work against gravity. Generally, the addition of slipping faults reduces the work required to accommodate tectonic strain. We see large differences in work energy saved by the addition of faults depending on fault rheology. Systems requiring less work are considered more efficient than those requiring greater work, and the system requiring a minimum of work would be favored under efficiency considerations. Calculations of minimum work deformation are shown to match expected deformation paths, indicating the usefulness of this approach for evaluating efficiency in more complex systems. A work balance approach to examining fault systems holds great potential for allowing analysis of entire systems of interacting faults and understanding fault system evolution.

[63] **Acknowledgments.** This manuscript greatly benefited from our discussions from Gautam Mitra, Heather Savage, and Jon Lewis as well as from comments of two anonymous reviewers. Graduate fellowships from both the University of Massachusetts Graduate School and the National Science Foundation provided support for Susan Murphy.

References

Abercrombie, R. E. (1995), Earthquake source scaling relationships from –1 to 5 M (sub L) using seismograms recorded at 2.5-km depth, *J. Geophys. Res.*, *100*, 24,015–24,036.

Argus, D. F., et al. (1999), Shortening and thickening of metropolitan Los Angeles measured and inferred by using geodesy, *Geology*, *27*, 703–706.

Bawden, G. W., W. Thatcher, R. S. Stein, K. W. Hudnut, and G. Peltzer (2001), Tectonic contraction across Los Angeles after removal of groundwater pumping effects, *Nature*, *412*, 812–815.

Buczkowski, D. L., and M. L. Cooke (2004), Formation of double-ring circular grabens due to volumetric compaction over buried impact craters: Implications for thickness and nature of cover material in Utopia Planitia, Mars, *J. Geophys. Res.*, *109*, E02006, doi:10.1029/2003JE002144.

Byerlee, J. D. (1978), Friction of rocks, *Pure Appl. Geophys.*, *119*, 615–626.

Childs, C., et al. (2003), The growth and propagation of synsedimentary faults, *J. Struct. Geol.*, *25*, 633–648.

Cohen, S. (1984), Crustal deformation, the earthquake cycle, and models of viscoelastic flow in the asthenosphere, *Geophys. J. R. Astron. Soc.*, *78*, 735–750.

Cooke, M. L., and A. Kameda (2002), Mechanical fault interaction within the Los Angeles Basin: A two-dimensional analysis using mechanical efficiency, *J. Geophys. Res.*, *107*(B7), 2146, doi:10.1029/2001JB000542.

Cooke, M., and D. Pollard (1997), Bedding-plane slip in initial stages of fault-related folding, *J. Struct. Geol.*, *19*, 567–581.

Cooke, M., and C. Underwood (2001), Fracture termination and step-over at bedding surfaces due to frictional slip and interface debonding, *J. Struct. Geol.*, *23*, 223–238.

Cooke, M., P. Mollema, D. Pollard, and A. Aydin (2000), Interlayer slip and joint localization in East Kaibab Monocline, Utah: Field evidence and results from numerical modeling, in *Forced Folds and Associated Frac-*

tures, edited by J. W. Cosgrove and M. S. Ameen, *Geol. Soc. Spec. Publ.*, *169*, 23–49.
Cox, S. J. D., and C. H. Scholz (1988), Rupture initiation in shear fracture of rocks: An experimental study, *J. Geophys. Res.*, *93*, 3307–3320.
Crouch, S. L., and A. M. Starfield (1990), *Boundary Element Methods in Solid Mechanics*, Unwin Hyman, Boston, Mass.
Dahlen, F. A., and T. D. Barr (1989), Brittle frictional mountain building: 1. Deformation and mechanical energy budget, *J. Geophys. Res.*, *94*, 3906–3922.
Davis, T. L., J. Namson, and R. F. Yerkes (1989), A cross section of the Los Angeles area; seismically active fold and thrust belt, the 1987 Whittier Narrows earthquake, and earthquake hazard, *J. Geophys. Res.*, *94*, 9644–9664.
Dawers, N. H., and J. R. Underhill (2000), The role of fault interaction and linkage in controlling synrift stratigraphic sequences: Late Jurassic, Statfjord East area, northern North Sea, *AAPG Bull.*, *84*(1), 45–64.
Deng, J., and L. R. Sykes (1997), Evolution of the stress field in southern California and triggering of moderate-sized earthquakes: A 200-year perspective, *J. Geophys. Res.*, *102*, 9859–9886.
Dieterich, J. H. (1979), Modeling of rock friction: 1. Experimental results and constitutive equations, *J. Geophys. Res.*, *84*, 2161–2168.
Du, Y., and A. Aydin (1993), The maximum distortional strain energy density criterion for shear fracture propagation with applications to the growth paths of en echelon faults, *Geophys. Res. Lett.*, *20*, 1091–1094.
Engelder, T. (1993), *Stress Regimes in the Lithosphere*, Princeton Univ. Press, Princeton, N. J.
Goodman, R. (1989), *Introduction to Rock Mechanics*, 2nd ed., 562 pp., John Wiley, Hoboken, N. J.
Griffith, W. A., and M. Cooke (2004), Mechanical validation of the three-dimensional intersection geometry between the Puente Hills blind thrust system and the Whittier fault, Los Angeles, CA, *Bull. Seismol. Soc. Am.*, *94*, 493–505.
Gupta, S., P. A. Cowie, N. H. Dawers, and J. R. Underhill (1998), A mechanism to explain rift-basin subsidence and stratigraphic patterns through fault array evolution, *Geology*, *26*, 595–598.
Handin, J. (1966), Strength and ductility, in *Handbook of Physical Constants*, edited by J. S. P. Clark, *Mem. Geol. Soc. Am.*, *97*, 223–290.
Harris, R. A. (1998), Stress triggers, stress shadows, and implications for seismic hazard, Introduction to the special issue, *J. Geophys. Res.*, *103*, 24,347–24,358.
Jaeger, J. C., and N. G. W. Cook (1976), *Fundamentals of Rock Mechanics*, John Wiley, Hoboken, N. J.
Jamison, W. R. (1993), Mechanical stability of the triangle zone; the backthrust wedge, *J. Geophys. Res.*, *98*, 20,105–20,030.
Kattenhorn, S. A., and D. D. Pollard (2001), Integrating 3–D seismic data, field analogs, and mechanical models in the analysis of segmented normal faults in the Wytch Farm oil field, southern England, United Kingdom, *AAPG Bull.*, *85*(7), 1183–1210.
King, G. C. P., R. S. Stein, and J. Lin (1994), Static stress changes and the triggering of earthquakes, *Bull. Seismol. Soc. Am.*, *84*(3), 935–953.
Lawn, B. R., and T. R. Wilshaw (1975), *Fracture of Brittle Solids*, Cambridge Univ. Press, New York.
Maerten, L., E. J. M. Willemse, D. D. Pollard, and K. Rawnsley (1999), Slip distributions on intersecting normal faults, *J. Struct. Geol.*, *21*(3), 259–271.
Mansfield, C., and J. Cartwright (2001), Fault growth by linkage: Observation and implications from analogue models, *J. Struct. Geol.*, *23*, 745–763.
Marone, C. (1998), Laboratory-derived friction laws and their application to seismic faulting, *Annu. Rev. Earth Planet Sci.*, *26*, 643–696.
Masek, J. G., and C. C. Duncan (1998), Minimum-work mountain building, *J. Geophys. Res.*, *103*, 907–917.
McGarr, A. (1994), Some comparisons between mining-induced and laboratory earthquakes, *Pure Appl. Geophys.*, *142*, 467–489.
McGarr, A. (1999), On relating apparent stress to the stress causing earthquake fault slip, *J. Geophys. Res.*, *104*, 3003–3011.
Mitra, G., and S. E. Boyer (1986), Energy balance and deformation mechanisms of duplexes, *J. Struct. Geol.*, *8*, 291–304.
Molnar, P., and H. Lyon-Caen (1988), Some simple physical aspects of the support, structure, and evolution of mountain belts, in *Processes in Continental Lithospheric Deformation*, edited by S. P. Clark Jr., C. B. Burchfiel, and J. Suppe, *Spec. Pap. Geol. Soc. Am.*, *218*, 197–207.
Nino, F., H. Philip, and J. Chery (1998), The role of bed-parallel slip in the formation of blind thrust faults, *J. Struct. Geol.*, *20*, 503–516.
Robertson, E. C. (1983), Relationship of fault-displacement to gouge and breccia thickness, *Min. Eng.*, *35*, 1426–1432.
Roering, J., M. Cooke, and D. D. Pollard (1997), Why blind thrust faults don't propagate to the Earth's surface: Numerical modeling of coseismic deformation associated with thrust-related anticlines, *J. Geophys. Res.*, *102*, 11,901–11,912.
Rundle, J. (1982), Viscoelastic-gravitational deformation by a rectangular thrust fault in a layered Earth, *J. Geophys. Res.*, *87*, 7787–7796.
Savage, H. M., and M. L. Cooke (2004), An investigation into the role of fault interaction on fold pattern, *J. Struct. Geol.*, *26*, 905–917.
Scholz, C. H. (1987), Wear and gouge formation in brittle faulting, *Geology*, *15*, 493–495.
Scholz, C. H. (2000), Evidence for a strong San Andreas fault, *Geology*, *28*(2), 163–166.
Scholz, C. H. (2002), *The Mechanics of Earthquakes and Faulting*, Cambridge Univ. Press, New York.
Shaw, J. H., and J. Suppe (1996), Earthquake hazard of active blind-thrust faults under the central Los Angeles basin, California, *J. Geophys. Res.*, *101*, 8623–8642.
Shen, Z. K., D. D. Jackson, and B. X. Ge (1996), Crustal deformation across and beyond the Los Angeles Basin from geodetic measurements, *J. Geophys. Res.*, *101*, 27,957–27,980.
Sleep, N. H., S. Stein, R. J. Geller, and R. G. Gordon (1979), The use of the minimum-dissipation principle in tectonophysics: Discussion, *Earth Planet. Sci. Lett.*, *45*(1), 218–220.
Stein, R. S. (1999), The role of stress transfer in earthquake occurrence, *Nature*, *402*, 605–609.
Timoshenko, S. P., and J. N. Goodier (1934), *Theory of Elasticity*, McGraw-Hill, New York.
Walls, C., T. Rockwell, K. Mueller, Y. Bock, S. Williams, J. Pfanner, J. Dolan, and P. Fang (1998), Escape tectonics in the Los Angeles metropolitan region and implications for seismic risk, *Nature*, *364*, 356–360.
Willemse, E. J. M., and D. D. Pollard (2000), Normal fault growth: Evolution of tipline shapes and slip distribution, in *Aspects of Tectonic Faulting*, edited by edited by F. K. Lehner and J. L. Urai, pp. 193–226, Springer-Verlag, New York.
Wong, T. F. (1982), Shear fracture energy of Westerly granite from post-failure behavior, *J. Geophys. Res.*, *87*, 990–1000.
Wong, T. F. (1986), On the normal stress dependence of the shear fracture energy, in *Earthquake Source Mechanics*, *Geophys. Monogr. Ser.*, vol. 37, edited by S. Das, J. Boatwright, and C. Scholz, pp. 1–12, AGU, Washington, D. C.
Wright, T. L. (1991), Structural geology and tectonic evolution of the Los Angeles Basin, California, in *Active Margin Basins*, edited by K. T. Biddle, *AAPG Mem.*, *52*, 35–134.
Yerkes, R. F. (1965), Geology of the Los Angeles Basin, California: An introduction, *U.S. Geol. Surv. Prof. Pap.*, *0420–A*, A1–A57.
Young, H. D., and R. A. Freedman (1996), *University Physics*, 9th ed., Addison-Wesley, Reading, Mass.

M. L. Cooke and S. Murphy, Geosciences Department, University of Massachusetts, Amherst, MA 01003, USA. (cooke@geo.umass.edu)